

## **Supporting Information**

# **Non-Directed C–H/C–F Coupling for the Synthesis of $\alpha$ -Fluoro Olefinated Arenes**

Sandip Porey, Yogesh Bairagi, Srimanta Guin, Xinglong Zhang<sup>2,\*</sup> & Debabrata Maiti<sup>1,\*</sup>

<sup>1</sup>Department of Chemistry, Indian Institute of Technology Bombay, Powai, Mumbai 400076, India

<sup>2</sup>Institute of High Performance Computing (IHPC), Agency for Science, Technology and Research (A\*STAR), 1 Fusionopolis Way, #16-16 Connexis, Singapore 138632, Republic of Singapore

E-mail: [dmaiti@chem.iitb.ac.in](mailto:dmaiti@chem.iitb.ac.in)

E-mail: [zhang\\_xinglong@ihpc.a-star.edu.sg](mailto:zhang_xinglong@ihpc.a-star.edu.sg)

## 8. Computational Methods.

Density functional theory (DFT) calculations were performed with Gaussian 16 rev. B.01.<sup>1</sup> Geometry optimizations were initially performed using the global-hybrid meta-NGA (nonseparable gradient approximation) MN15 functional<sup>2</sup> with the def2-SVP<sup>3,4</sup> Karlsruhe-family basis set and the optimized structures further refined with a mix of larger basis set consisting of triple- $\zeta$  valence def2-TZVPPD (where ‘D’ indicates diffuse basis functions) for Pd<sup>5,6</sup> and Cu<sup>5,6</sup> and Br<sup>5</sup> atom and def2-SVP<sup>3,4</sup> for all other atoms (BS1). Minima and transition structures on the potential energy surface (PES) were confirmed using harmonic frequency analysis at the same level of theory, showing respectively zero and one imaginary frequency. Where appropriate for cases where visual inspection of TS imaginary frequency is not obvious, intrinsic reaction coordinate (IRC) analyses<sup>7,8</sup> were performed to confirm that the found TSs connect to the right reactants and products.

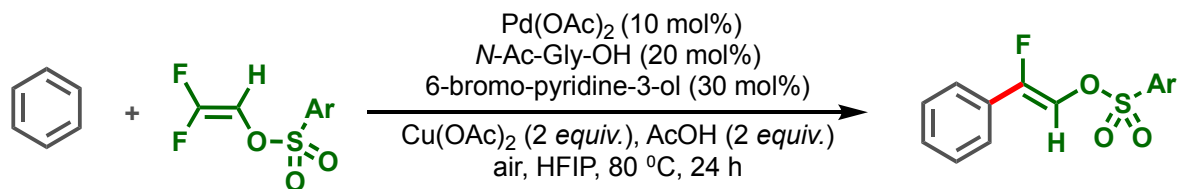
Single point (SP) corrections were performed using MN15 functional and def2-QZVP<sup>3</sup> basis set for all atoms. The SMD implicit continuum solvation model<sup>9</sup> was used to account for the effect of hexafluoroisopropanol (HFIP) solvent on the computed Gibbs energy profile. Since HFIP solvent is not available in the list of default/pre-defined solvents in the Gaussian 16 software, it is herein parametrised using a set of seven parameters.<sup>9</sup> These include 1) the static dielectric constant of the solvent at 25°C (Eps = 16.7);<sup>10-12</sup> 2) dynamic (optical) dielectric constant – the square of the refractive index value of 1.275 at 20°C was used<sup>13</sup> (EpsInf = 1.625625); 3) hydrogen bond acidity (HBondAcidity = 0.77)<sup>14</sup> and 4) hydrogen bond basicity (HBondBasicity = 0.10)<sup>14</sup>, which are Abraham’s A and B values respectively; 5) the surface tension of the solvent at interface (SurfaceTensionAtInterface = 23.23)<sup>15</sup> – this value is obtained from the conversion of the surface tension of HFIP at 16.14 mN/m at 25°C<sup>16</sup> to cal mol<sup>-1</sup> Å<sup>-2</sup> used in the SMD model by the conversion factor of 1 dyne/cm = 1 mN/m = 1.43932 cal mol<sup>-1</sup> Å<sup>-2</sup> as outlined in the Truhlar’s Minnesota Solvent Descriptor Database<sup>17</sup>; 6) carbon aromaticity – the fraction of aromatic carbons (CarbonAromaticity = 0.00) and 7) electronegative halogenicity – the fraction of halogens (Electronegative Halogenicity = 0.60). These parameters were specified using the keyword “SCRF = (SMD, Solvent= Generic, Read)” in Gaussian 16.

Gibbs energies were evaluated at the reaction temperature of 353.15 K (80°C), using a quasi-RRHO treatment of vibrational entropies.<sup>18,19</sup> Vibrational entropies of frequencies below 100 cm<sup>-1</sup> were obtained according to a free rotor description, using a smooth damping function to interpolate between the two limiting descriptions. The free energies were further corrected using standard concentration of 1 mol/L, which were used in solvation calculations. Unless otherwise stated, the final SMD

(dichloroethane)-MN15/def2-QZVP//MN15/BS1 Gibbs energies are used for discussion throughout. All Gibbs energy values in the text and figures are quoted in kcal mol<sup>-1</sup>. *All molecular structures and molecular orbitals were visualized using PyMOL software.*<sup>20</sup>

### 8.1. Model reaction

For computational modeling, we have chosen the following reaction, where benzene was used as a substrate (Scheme S1), for mechanistic studies.

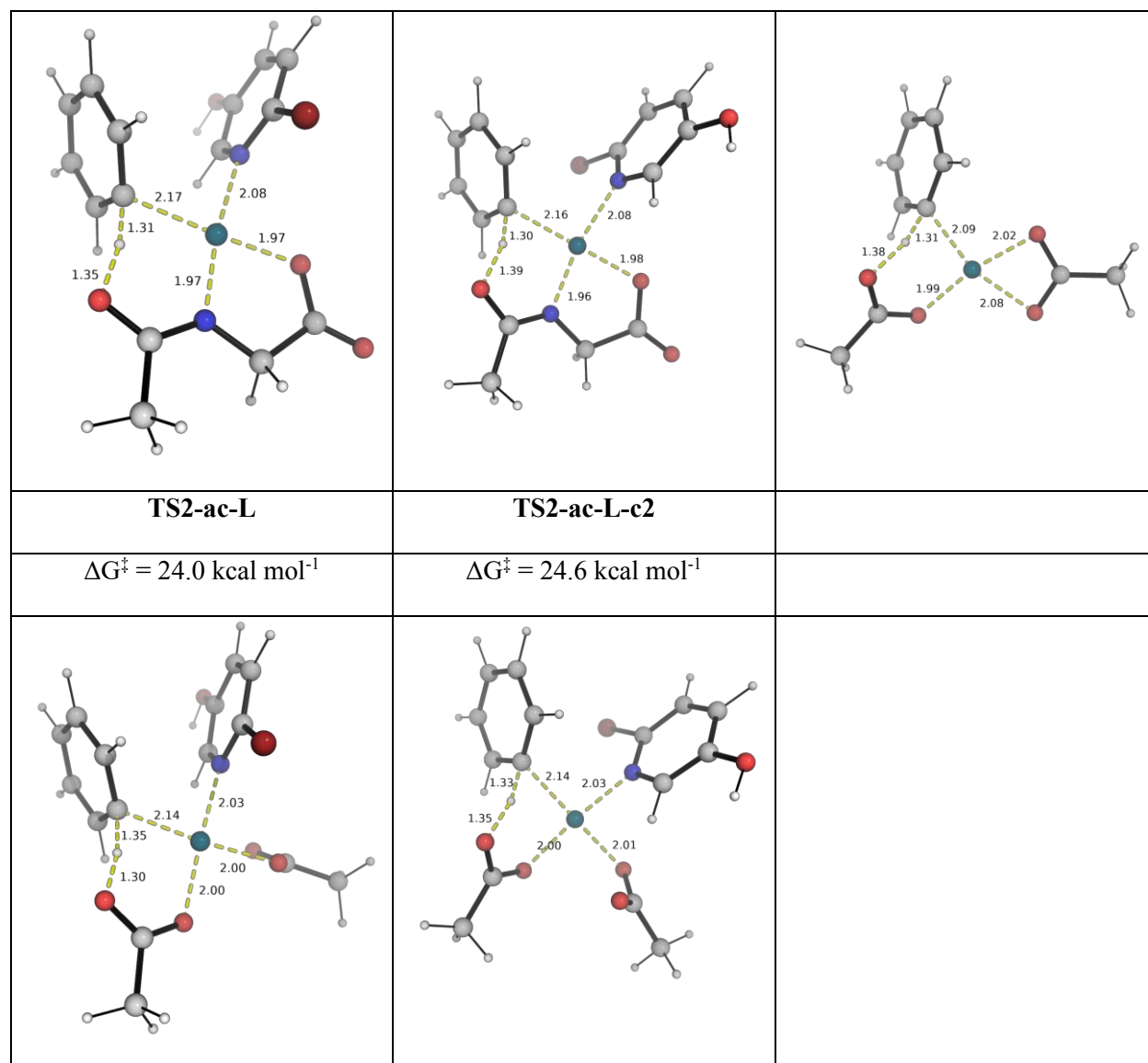


**Scheme S1.** Model reaction used for computational mechanistic studies.

### 8.2. C–H activation transition states (TSs)

The roles of the ligands were considered computationally in the step of C–H activation. The DFT-optimized TS structures are shown in Figure S1. Conformations where the ligands are oriented differently were also considered. The C–H activation using MPAA ligand as the base in carrying out the concerted metalation deprotonation, with one molecule of 6-bromo-pyridine-3-ol coordinated to Pd-center, via **TS2**, has the lowest activation barrier. Using only the acetate ligand without 6-bromo-pyridine-3-ol or MPAA ligand for C–H activation, via **TS2-ac**, gives a much higher barrier, by 7.4 kcal mol<sup>-1</sup>; on the other hand, using the acetate ligand in the presence of 6-bromo-pyridine-3-ol coordinate, **TS2-ac-L**, lowers the barrier to 24.0 kcal mol<sup>-1</sup>, however, it is still 5.6 kcal mol<sup>-1</sup> higher than **TS2**. Thus, the involvement of MPAA as the base to carry out C–H activation is much more kinetically favorable.

<b>TS2</b>	<b>TS2-c2</b>	<b>TS2-ac</b>
$\Delta G^\ddagger = 18.4 \text{ kcal mol}^{-1}$	20.5 kcal mol <sup>-1</sup>	25.8 kcal mol <sup>-1</sup>

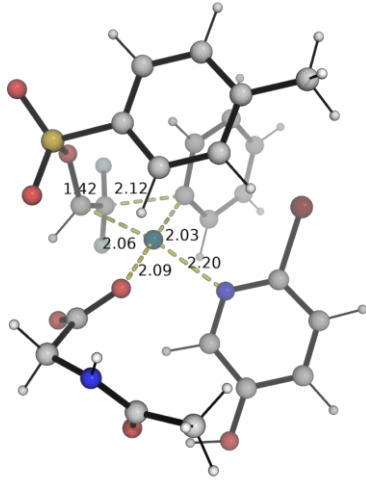
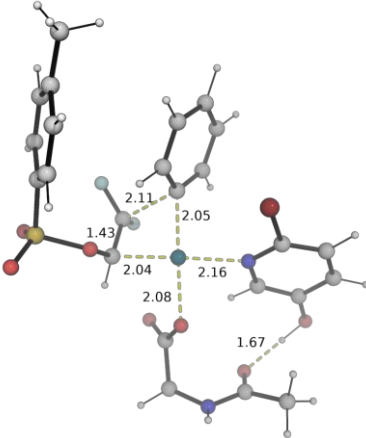
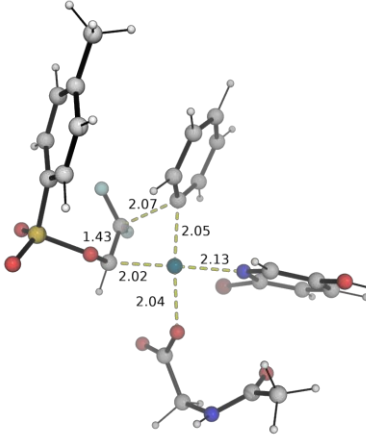
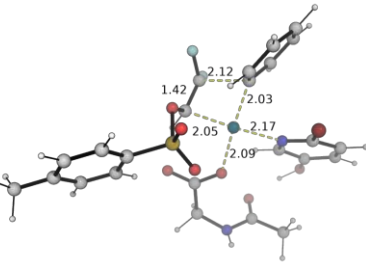
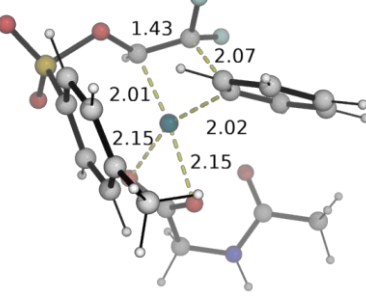
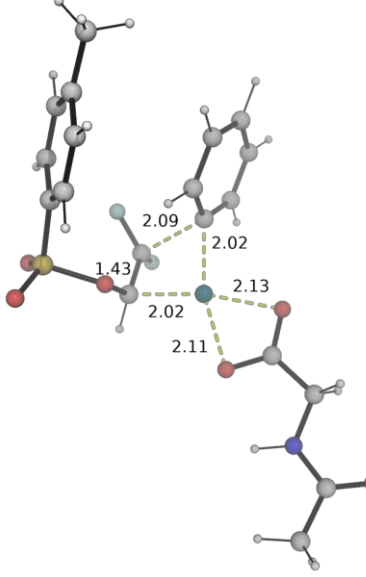


**Figure S1.** DFT optimized transition state structures for the C–H activation of substrate using different ligands. Activation barriers are taken relative to the sum of starting materials.

### 8.3. Carbopalladation

After C–H activation by MPAA ligand, the resulting ligand occurs in imidic acid form. We computationally investigated the energetics of the MPAA ligand in imidic acid vs its tautomeric amide form for subsequent  $\beta$ -F elimination. The DFT optimized structures and the associated activation barriers are given in Figure S2.

We note that the occurrence of MPAA ligand in imidic acid form (**TS3-im**, **TS3-im-c2** and **TS3-im-L**) all give higher activation barriers than the corresponding amide form (e.g., **TS3-im-L** compared to **TS3-c3** and **TS3-im-c2** compared to **TS3-noL-c2**).

<b>TS3</b>	<b>TS3-c2</b>	<b>TS3-c3</b>
$\Delta G^\ddagger = 16.5 \text{ kcal mol}^{-1}$	21.4 kcal mol <sup>-1</sup>	22.2 kcal mol <sup>-1</sup>
		
<b>TS3-c4</b>	<b>TS3-noL</b>	<b>TS3-noL-c2</b>
$\Delta G^\ddagger = 22.9 \text{ kcal mol}^{-1}$	19.1 kcal mol <sup>-1</sup>	22.2 kcal mol <sup>-1</sup>
		
<b>TS3-im</b>	<b>TS3-im-c2</b>	<b>TS3-im-L</b>
24.2 kcal mol <sup>-1</sup>	$\Delta G^\ddagger = 37.5 \text{ kcal mol}^{-1}$	39.0 kcal mol <sup>-1</sup>

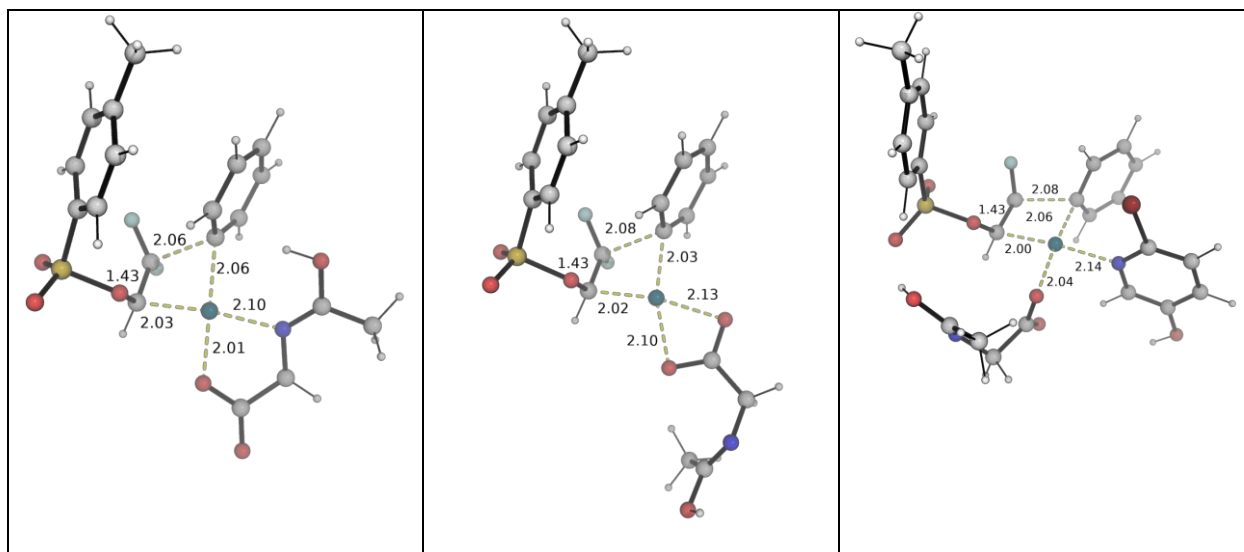


**Figure S2.** DFT optimized transition state structures for the carbopalladation step involving different ligands. Note that the MPAA ligand can occur in either imidic acid form (**TS3-im**, **TS3-im-c2** and **TS3-im-L**) or amide form form (**TS3** and **TS3-c2**). Activation barriers are taken relative to the sum of starting materials.

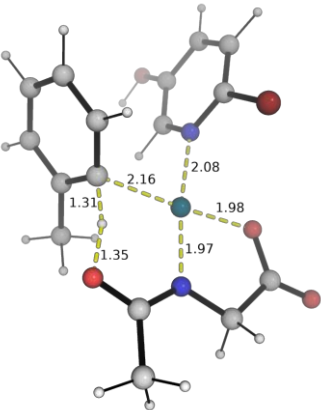
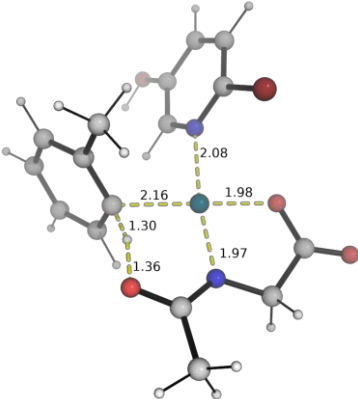
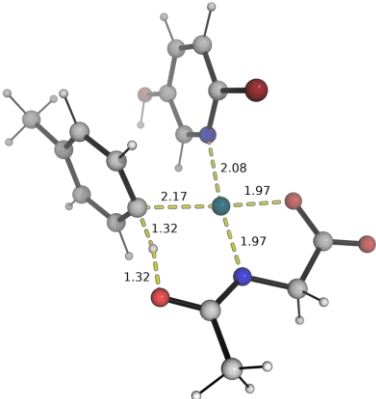
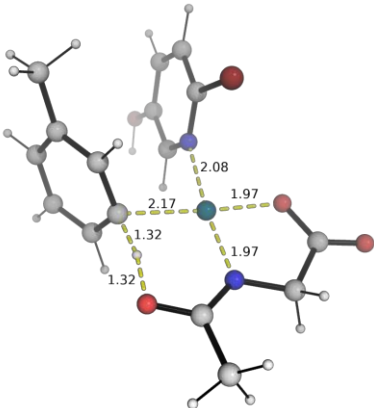
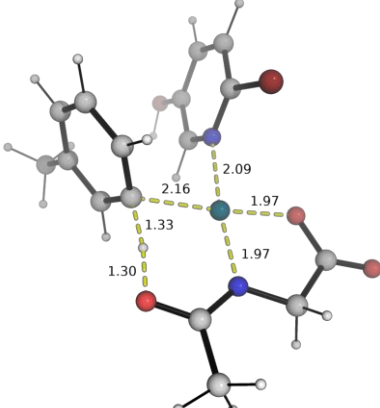
#### 8.4. Regioselectivity studies for selected substrates

We performed computational studies on the regioselectivity outcomes using toluene and *tert*-butylbenzene substrates (giving rise to the formation of product **5** and product **7**, respectively) by focusing on the turnover-frequency determining step (C–H activation step). Figures S3 and S4 show the DFT optimized TS structures and the relative activation barriers, taking the TS with the lowest barrier within each substrate as reference zero. All 5 possible sites for C–H activation were considered, such that two conformers exist for the C–H activation of *ortho*- and *meta*-sites.

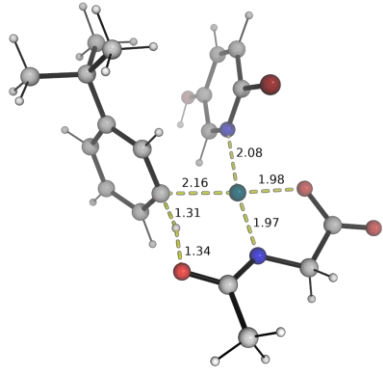
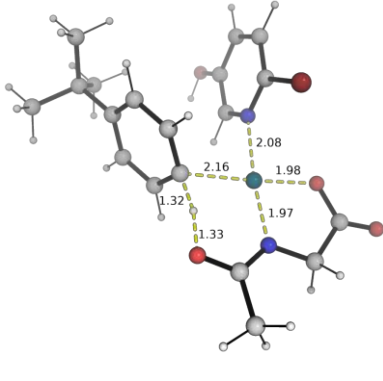
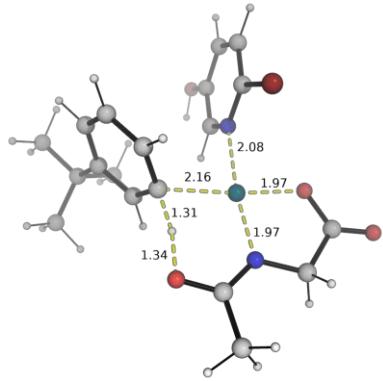
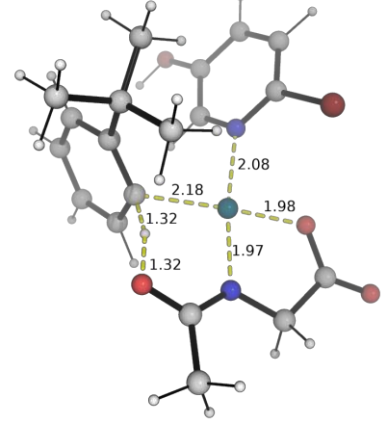
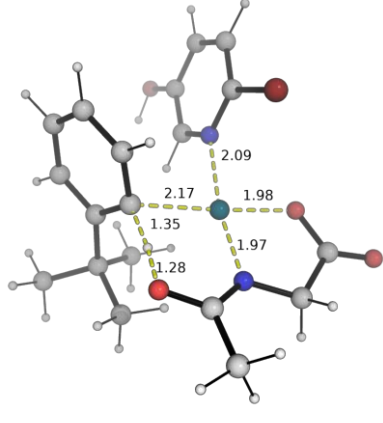
For toluene substrate, we see that the activation of either *ortho*-sites have the lowest barrier than *para*- and *meta*-activation (Figure S3). The activation of *ortho*-site has 1.2 kcal mol<sup>-1</sup> lower barrier than *para*-activation and *meta*-activation. This gives an estimated selectivity ratio of 5.5:1:1 for *ortho:para:meta* using simple transition state theory. Our selectivity studies agrees qualitatively well with the experimental observation favouring *ortho*-activation.

For *tert*-butylbenzene substrate, we see that the activation of *meta*-site (**m-TS2-tbu**) has the lowest barrier while the activation of *para*-site (**p-TS2-tbu**) has a barrier of 0.5 kcal mol<sup>-1</sup> higher whereas the activation of *ortho*-site (**o-TS2-tbu**) has a barrier of  $\Delta\Delta G^\ddagger = 3.0$  kcal mol<sup>-1</sup>. This predicts a selectivity of 1:2:72 for *meta:para:ortho*, if simple transition state theory correlates with experimental observation perfectly. We note that the barrier difference of 0.5 kcal mol<sup>-1</sup> between **m-TS2-tbu** and **p-TS2-tbu** is rather small and may fall within the accuracy of the level of theory, however, we note that the prediction

of  $\Delta\Delta G^\ddagger$  may benefit from error cancellations. Nevertheless, the ortho site is much less favoured than the meta site, very much likely due to the unfavourable steric clashes with the the other side groups present in the transition state structures (Figure S4).

<b>o-TS2-tol</b>	<b>o-TS2-tol-c2</b>	<b>p-TS2-tol</b>
$\Delta\Delta G^\ddagger = 0.0 \text{ kcal mol}^{-1}$	$0.8 \text{ kcal mol}^{-1}$	$1.2 \text{ kcal mol}^{-1}$
		
<b>m-TS2-tol</b>	<b>m-TS2-tol-c2</b>	
$\Delta\Delta G^\ddagger = 1.2 \text{ kcal mol}^{-1}$	$2.2 \text{ kcal mol}^{-1}$	
		

**Figure S3.** DFT optimized transition state structures for the C–H activation of toluene substrate. Relative activation barriers are taken with reference to the TS with the lowest Gibbs energy.

<b>m-TS2-tbu</b>	<b>p-TS2-tbu</b>	<b>m-TS2-tbu-c2</b>
$\Delta\Delta G^\ddagger = 0.0 \text{ kcal mol}^{-1}$	$0.5 \text{ kcal mol}^{-1}$	$1.3 \text{ kcal mol}^{-1}$
		
<b>o-TS2-tbu</b>	<b>o-TS2-tbu-c2</b>	
$\Delta\Delta G^\ddagger = 3.0 \text{ kcal mol}^{-1}$	$4.3 \text{ kcal mol}^{-1}$	
		

**Figure S4.** DFT optimized transition state structures for the C–H activation of tert-butylbenzene substrate. Relative activation barriers are taken with reference to the TS with the lowest Gibbs energy.

### 8.5. E/Z selectivity outcome studies for selected substrates

We performed computational studies on the  $\beta$ -F elimination step (**TS4**) to understand the *E/Z* selectivity outcome in the product using benzene and 1,3-diisopropyl-2-methoxybenzene substrates (giving rise to the formation of product **4** and product **25**, respectively). Figures S5 and S6 show the DFT optimized TS structures (including conformers of the TSs) and the relative activation barriers, taking the TS with the lowest barrier within each substrate as reference zero. After consideration of different conformers, we found that the *Z*-product, formed via **TS4**, is favoured over the *E*-product, formed via **TS4'**, by 1.0



kcal mol<sup>-1</sup>, suggesting that the *Z*:*E* product formed (product **4**) will have a ratio of roughly 4:1, when benzene substrate is used.

<b>TS4</b>	<b>TS4-c2</b>	<b>TS4-c3</b>
$\Delta\Delta G^\ddagger = 0.0$ kcal mol <sup>-1</sup>	0.3 kcal mol <sup>-1</sup>	0.6 kcal mol <sup>-1</sup>
<b>TS4-c4</b>	<b>TS4-c5</b>	<b>TS4-c6</b>
$\Delta\Delta G^\ddagger = 1.2$ kcal mol <sup>-1</sup>	1.4 kcal mol <sup>-1</sup>	1.8 kcal mol <sup>-1</sup>
<b>TS4'</b>	<b>TS4'-c2</b>	<b>TS4'-c3</b>
$\Delta\Delta G^\ddagger = 1.0$ kcal mol <sup>-1</sup>	2.1 kcal mol <sup>-1</sup>	3.0 kcal mol <sup>-1</sup>

**Figure S5.** DFT optimized transition state structures for the  $\beta$ -F elimination step using benzene substrate. Relative activation barriers are taken with reference to the TS with the lowest Gibbs energy.

We further consider the *E/Z* selectivity outcome when 1,3-diisopropyl-2-methoxybenzene is used. Taking the lowest energy conformers from benzene substrate (**TS4** vs **TS4'**) and modifying accordingly for TS search, we note that the formation of the *Z*-product (product **25**), formed via **TS4a**, is favoured over the *E*-product, formed via **TS4a'**, by 5.3 kcal mol<sup>-1</sup> (Figure S6), translating to a *Z:E* ratio of ~1906:1, thus suggesting that product **25** formed will predominantly have the *Z*-stereochemistry across C=C double bond, consistent with the X-ray crystal structure obtained for product **25**.

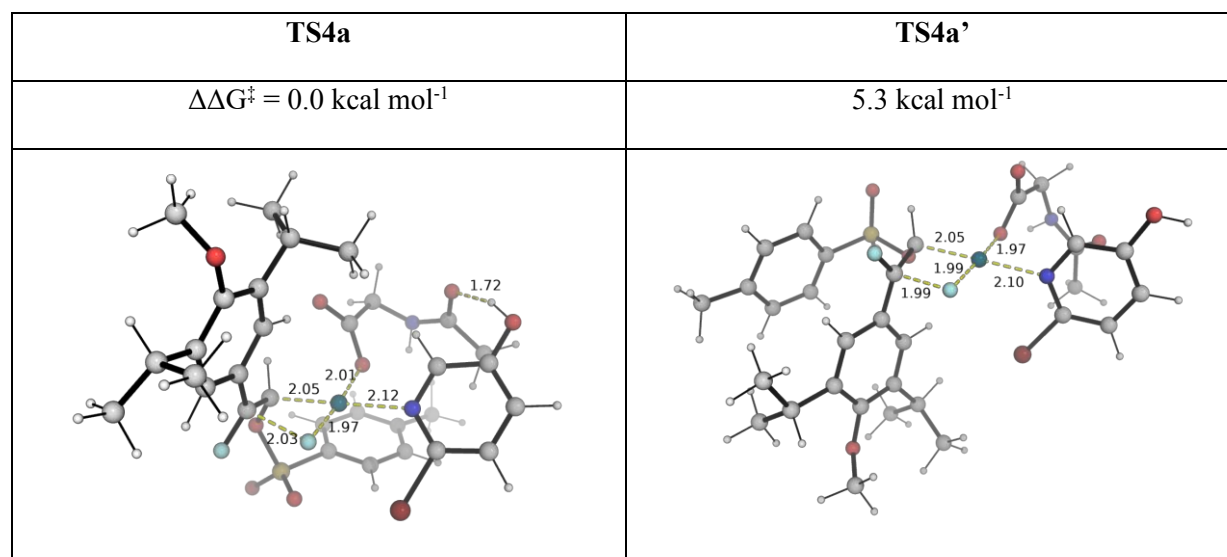


**Figure S6.** DFT optimized transition state structures for the  $\beta$ -F elimination step using 1,3-diisopropyl-2-methoxybenzene substrate. Relative activation barriers are taken with reference to the TS with the lowest Gibbs energy.

### 8.6. Optimized structures and absolute energies, zero-point energies

Geometries of all optimized structures (in .xyz format with their associated energy in Hartrees) are included in a separate folder named *DFT\_optimized\_structures*. All these data have been deposited and uploaded to zenodo.org <https://zenodo.org/record/8003075> (DOI: 10.5281/zenodo.8003075).

Absolute values (in Hartrees) for SCF energy, zero-point vibrational energy (ZPE), enthalpy and quasi-harmonic Gibbs free energy (at 80°C/353.15 K) for optimized structures are given below. Single point corrections in SMD hexafluoroisopropanol using MN15/def2-QZVP level of theory are also included.

<b>Structure</b>	<b>E/au</b>	<b>ZPE/au</b>	<b>H/au</b>	<b>T.S/au</b>	<b>qh-G/au</b>	<b>SP MN15/def2- QZVP</b>
<b>HOAc</b>	-228.644533	0.062197	-228.57532	0.036449	-228.611431	-229.06457600
<b>acetate</b>	-228.059294	0.048219	-228.00424	0.037042	-228.04024	-228.592055

<b>Nacetylglycine</b>	-436.253431	0.118206	-436.12243	0.053247	-436.17305	-437.053674
<b>bromopyridinol</b>	-2896.411538	0.083581	-2896.3178	0.046192	-2896.363813	-2897.490168
<b>benzene</b>	-231.75014	0.101235	-231.64172	0.037091	-231.678816	-232.179563
<b>difluoroalkene</b>	-1169.50093	0.161883	-1169.3189	0.072129	-1169.386533	-1171.169628
<b>HF</b>	-100.265732	0.009533	-100.25229	0.020247	-100.272533	-100.461549
<b>PdOAc<sub>2</sub> monomer</b>	-583.809931	0.104326	-583.69077	0.058992	-583.746969	-584.634037
<b>INT1</b>	-1020.111598	0.224275	-1019.8601	0.088211	-1019.942688	-1021.717401
<b>TS1</b>	-1020.104362	0.220761	-1019.8571	0.087306	-1019.938316	-1021.706512
<b>INT2</b>	-1020.104385	0.222157	-1019.855	0.089402	-1019.937836	-1021.706943
<b>INT1-c2</b>	-1020.10387	0.224082	-1019.8525	0.088685	-1019.935244	-1021.71199
<b>TS1-c2</b>	-1020.100387	0.219985	-1019.8538	0.086353	-1019.934852	-1021.702892
<b>INT2-c2</b>	-1020.104016	0.224274	-1019.8527	0.087811	-1019.934812	-1021.706684
<b>INT3</b>	-6356.305365	0.266449	-6356.0038	0.108461	-6356.103356	-6358.573781
<b>INT3-c2</b>	-6356.313302	0.267026	-6356.0114	0.106012	-6356.109691	-6358.574531
<b>INT3-c3</b>	-6356.308242	0.2668	-6356.0065	0.106085	-6356.104969	-6358.574061
<b>INT3-c4</b>	-6356.307011	0.266625	-6356.0053	0.106533	-6356.104014	-6358.573319
<b>INT4</b>	-3691.288223	0.283845	-3690.9723	0.098699	-3691.064741	-3693.243134
<b>TS2</b>	-3691.272552	0.278543	-3690.9623	0.098563	-3691.054114	-3693.22125
<b>TS2-c2</b>	-3691.270153	0.278676	-3690.9599	0.097464	-3691.051172	-3693.218358
<b>TS2-ac</b>	-815.540969	0.201142	-815.31725	0.077188	-815.389973	-816.789197
<b>TS2-ac-L</b>	-3712.327462	0.286196	-3712.0073	0.105427	-3712.103972	-3714.307054
<b>TS2-ac-L-c2</b>	-3712.328422	0.286708	-3712.0081	0.102337	-3712.103565	-3714.30741
<b>INT5</b>	-3691.298339	0.284276	-3690.9819	0.099962	-3691.074439	-3693.251051
<b>INT6</b>	-4860.835893	0.446785	-4860.3358	0.14857	-4860.470676	-4864.439343
<b>TS3</b>	-4860.83962	0.447696	-4860.3406	0.139901	-4860.470051	-4864.430666
<b>TS3-c2</b>	-4860.82502	0.447235	-4860.3261	0.143481	-4860.457272	-4864.420964
<b>TS3-c3</b>	-4860.81042	0.445804	-4860.312	0.146378	-4860.445095	-4864.417349
<b>TS3-c4</b>	-4860.83221	0.447484	-4860.3332	0.143312	-4860.464291	-4864.418744
<b>TS3-noL</b>	-1964.028041	0.361214	-1963.6259	0.117496	-1963.734802	-1966.907619

<b>TS3-noL-c2</b>	-1964.018807	0.360193	-1963.6168	0.124389	-1963.729502	-1966.898761
<b>TS3-im</b>	-1964.015667	0.361208	-1963.6136	0.11825	-1963.722833	-1966.899116
<b>TS3-im-c2</b>	-1963.996021	0.360961	-1963.5939	0.120612	-1963.704462	-1966.876631
<b>TS3-im-L</b>	-4860.787746	0.446756	-4860.2889	0.147056	-4860.421667	-4864.391249
<b>INT7</b>	-4860.884825	0.449893	-4860.3832	0.145137	-4860.514904	-4864.483842
<b>INT8</b>	-4860.875765	0.450103	-4860.3741	0.143827	-4860.505084	-4864.473787
<b>TS4</b>	-4860.838432	0.446919	-4860.3392	0.146574	-4860.472115	-4864.454916
<b>TS4-c2</b>	-4860.836403	0.447034	-4860.3372	0.145287	-4860.469617	-4864.453617
<b>INT9</b>	-4860.849853	0.448029	-4860.3488	0.148051	-4860.483109	-4864.4694
<b>INT10</b>	-3559.825795	0.196169	-3559.6033	0.086179	-3559.684398	-3561.531615
<b>product</b>	-1301.004239	0.251385	-1300.7277	0.079962	-1300.80399	-1302.92449

## 8.5. References:

### Full reference Gaussian 16:

Gaussian 16, Revision B.01, Frisch, M. J.; Trucks, G. W.; Schlegel, H. B.; Scuseria, G. E.; Robb, M. A.; Cheeseman, J. R.; Scalmani, G.; Barone, V.; Mennucci, B.; Petersson, G. A.; Nakatsuji, H.; Caricato, M.; Li, X.; Hratchian, H. P.; Izmaylov, A. F.; Bloino, J.; Zheng, G.; Sonnenberg, J. L.; Hada, M.; Ehara, M.; Toyota, K.; Fukuda, R.; Hasegawa, J.; Ishida, M.; Nakajima, T.; Honda, Y.; Kitao, O.; Nakai, H.; Vreven, T.; Montgomery Jr., J. A.; Peralta, J. E.; Ogliaro, F.; Bearpark, M.; Heyd, J. J.; Brothers, E.; Kudin, K. N.; Staroverov, V. N.; Kobayashi, R.; Normand, J.; Raghavachari, K.; Rendell, A.; Burant, J. C.; Iyengar, S. S.; Tomasi, J.; Cossi, M.; Rega, N.; Millam, J. M.; Klene, M.; Knox, J. E.; Cross, J. B.; Bakken, V.; Adamo, C.; Jaramillo, J.; Gomperts, R.; Stratmann, R. E.; Yazyev, O.; Austin, A. J.; Cammi, R.; Pomelli, C.; Ochterski, J. W.; Martin, R. L.; Morokuma, K.; Zakrzewski, V. G.; Voth, G. A.; Salvador, P.; Dannenberg, J. J.; Dapprich, S.; Daniels, A. D.; Farkas, Ö.; Foresman, J. B.; Ortiz, J. V.; Cioslowski, J.; Fox, D. J. Gaussian, Inc., Wallingford CT, 2016.

1. Frisch, M. J. .; Trucks, G. W. .; Schlegel, H. B. .; Scuseria, G. E. .; Robb, M. A. .; Cheeseman, J. R. .; Scalmani, G. .; Barone, V. .; Petersson, G. A. .; Nakatsuji, H. .; et al. Gaussian 16, Revision B.01. 2016.
2. Yu, H. S.; He, X.; Li, S. L.; Truhlar, D. G. MN15: A Kohn–Sham Global-Hybrid Exchange–Correlation Density Functional with Broad Accuracy for Multi-Reference and Single-

- Reference Systems and Noncovalent Interactions. *Chem. Sci.* **2016**, *7*, 5032–5051.
3. Weigend, F.; Ahlrichs, R. Balanced Basis Sets of Split Valence, Triple Zeta Valence and Quadruple Zeta Valence Quality for H to Rn: Design and Assessment of Accuracy. *Phys. Chem. Chem. Phys.* **2005**, *7*, 3297–3305.
  4. Weigend, F. Accurate Coulomb-Fitting Basis Sets for H to Rn. *Phys. Chem. Chem. Phys.* **2006**, *8*, 1057–1065.
  5. Rappoport, D.; Furche, F. Property-Optimized Gaussian Basis Sets for Molecular Response Calculations. *J. Chem. Phys.* **2010**, *133*, 134105.
  6. Andrae, D.; Häußermann, U.; Dolg, M.; Stoll, H.; Preuß, H. Energy-Adjusted ab Initio Pseudopotentials for the Second and Third Row Transition Elements. *Theor. Chim. Acta* **1990**, *77*, 123–141.
  7. Fukui, K. Formulation of the Reaction Coordinate. *J. Phys. Chem.* **2005**, *74*, 4161–4163.
  8. Fukui, K. The Path of Chemical Reactions - The IRC Approach. *Acc. Chem. Res.* **1981**, *14*, 363–368.
  9. Marenich, A. V.; Cramer, C. J.; Truhlar, D. G. Universal Solvation Model Based on Solute Electron Density and on a Continuum Model of the Solvent Defined by the Bulk Dielectric Constant and Atomic Surface Tensions. *J. Phys. Chem. B* **2009**, *113*, 6378–6396.
  10. Ebersson, L.; Hartshorn, M. P.; Persson, O.; Radner, F. Making Radical Cations Live Longer. *Chem. Commun.* **1996**, *18*, 2105–2112.
  11. Gu, X.; Song, X.; Shao, C.; Zeng, P.; Lu, X.; Shen, X.; Yang, Q. Electrospinning of Poly(Butylene-Carbonate): Effect of Solvents on the Properties of the Nanofibers Film. *Int. J. Electrochem. Sci.* **2014**, *9*, 8045–8056.
  12. Carraro, M.; Gardan, M.; Sartorel, A.; Maccato, C.; Bonchio, M. Hydrogen Peroxide Activation by Fluorophilic Polyoxotungstates for Fast and Selective Oxygen Transfer Catalysis. *Dalt. Trans.* **2016**, *45*, 14544–14548.
  13. Sigma-Aldrich. 1,1,1,3,3,3-Hexafluoro-2-propanol  
<https://www.sigmaaldrich.com/catalog/product/aldrich/105228> (accessed Jun 6, 2017).
  14. Abraham, M. H.; Andonian-Haftvan, J.; Whiting, G. S.; Leo, A.; Taft, R. S. Hydrogen Bonding. Part 34. The Factors That Influence the Solubility of Gases and Vapours in Water at 298 K, and a New Method for Its Determination. *J. Chem. Soc. Perkin Trans.* **1994**, *8*, 1777–

- 1791.
15. Richmond, E.; Yi, J.; Vuković, V. D.; Sajadi, F.; Rowley, C. N.; Moran, J. Ring-Opening Hydroarylation of Monosubstituted Cyclopropanes Enabled by Hexafluoroisopropanol. *Chem. Sci.* **2018**, *9*, 6411–6416.
  16. Berkessel, A.; Adrio, J. A. Dramatic Acceleration of Olefin Epoxidation in Fluorinated Alcohols: Activation of Hydrogen Peroxide by Multiple H-Bond Networks. *J. Am. Chem. Soc.* **2006**, *128*, 13412–13420.
  17. Winget, P.; Dolney, D. M.; Giesen, D. J.; Cramer, C. J.; Truhlar, D. G. Minnesota solvent descriptor database <https://comp.chem.umn.edu/solvation/mnsddb.pdf> (accessed Mar 15, 2022).
  18. Grimme, S. Supramolecular Binding Thermodynamics by Dispersion-Corrected Density Functional Theory. *Chem.: Eur. J.* **2012**, *18*, 9955–9964.
  19. Funes-Ardoiz, I.; Paton, R. S. GoodVibes v1.0.1 <http://doi.org/10.5281/zenodo.56091>.
  20. Schrödinger, L. *The PyMOL Molecular Graphics Development Component, Version 1.8*; 2015.